Available online at www.sciencedirect.com
ScienceDirect
Journal of Power Sources 163 (2007) 864–873
JOURNAL OF POWER SOURCES
www.elsevier.com/locate/jpowsour

# A two-fluid model for two-phase flow in PEMFCs

Guangli He [a], Pingwen Ming [b], Zongchang Zhao [a,*], Abuliti Abudula [c], Yu Xiao [b]

[a] *School of Chemical Engineering, Dalian University of Technology, Dalian 116012, PR China*
[b] *Fuel Cell R&D Center, Dalian Institute of Chemical Physics, Chinese Academy of Sciences, Dalian 116023, PR China*
[c] *New Energy Technology Research Division, Aomori Industrial Research Center, Aomori 030-0113, Japan*

Received 27 July 2006; received in revised form 26 September 2006; accepted 27 September 2006
Available online 13 November 2006

**Abstract**

In this study, a two-fluid (TF) model is developed for two-phase flows in proton exchange membrane fuel cells (PEMFCs). The drag force and lift force between gas and liquid phase are considered in N-S equations. In addition, a simplified model is introduced to obtain the liquid water droplet detachment diameter on the gas diffusion layer (GDL)/channel interface which involves the properties of the GDL/channel interface (contact angle and surface tension). The TF model and the simplified model for the prediction of water droplet detachment diameter on GDL/channel interface are validated by the comparison between the experimental data and the model results, respectively. The effect of the properties of GDL/channel interface (contact angle and surface tension) on two-phase behavior in PEMFCs is investigated, The results show that a high contact angle and a low surface tension are advantageous for liquid water removal in the gas channel and the GDL even though a low surface tension will lead to a low capillary force in the GDL.


*Keywords:* Fuel cell; PEMFCs; Two-fluid model; Two-phase flow; GDL/channel interface; Liquid water removal

## 1. Introduction

Proton exchange membrane fuel cells (PEMFCs) are regarded as the most promising energy conversion systems for future automobiles and stationary applications nowadays. Water management is the key issue in PEMFCs, and is a significant technical challenge. On the one hand, sufficient water is needed in the membrane to maintain sufficiently high proton conductivity, but on the other hand, excess liquid water in the electrode can cause 'flooding', and hinders the transport of the reactant from the gas channel to the catalyst layer. Liquid water transport in PEMFCs occurs as follows: (1) water is produced in cathode catalyst layer, and liquid water transports within the gas diffusion layer (GDL) by capillary-driven flow. (2) Liquid water droplets appear on the GDL/gas channel interface and are removed by the gas shearing function [1–4]. (3) Liquid water travels in the gas channel. Wang and co-workers [3] have observed the emergence, growth and detachment of liquid water droplet on the GDL/gas channel interface. Recently, they [5] have measured the size of the droplet on the GDL/gas channel interface, and find that liquid water can transport through the gas channel without interaction with channel wall at high gas velocity. Modeling liquid water behavior in PEMFCs will help to optimize the water management and the design of PEMFCs. At present, much modeling work has been done [6–12]. He et al. [6] developed a two-phase model of water transport in GDL for a two-dimensional cross-section of PEMFCs. They introduced a transport equation for liquid water in GDL which involved an advection term (due to bulk flow) and a diffusion term (due to capillary-driven flow). In Siegel's work [7], he assumed that the liquid phase had the same velocity with the gas phase, so the work is independent on the transport of liquid water in gas channel. He also considered the mass transfer in the catalyst layer in detail, which includes mass transfer among liquid phase, gas phase and polymer phase. Liu and co-workers [8–10] have employed the mixture model for two-phase behavior in PEMFCs, which can describe the liquid water behavior in GDL and gas channel with the advantages of simplicity and low cost of the calculation. Wang et al. [11] also introduced the mixture model to describe two-phase behavior in PEMFCs, and they predicted that the liquid water saturation within the cathode will reach 6.3% at 1.4 A $cm^{-2}$ for dry inlet air. In the continuation of this work, Wang and co-workers [12]

* Corresponding author. Tel.: +86 411 88993626.
*E-mail address:* zczhao55@163.com (Zongchang Zhao).

0378-7753/$ – see front matter © 2006 Elsevier B.V. All rights reserved.
doi:10.1016/j.jpowsour.2006.09.059

**Nomenclature**

| | |
|---|---|
| $C$ | concentration (mol cm$^{-3}$) |
| $C_L$ | lift coefficient |
| $C_{La}$ | constant for $C_L$ (0.2) |
| $d_c$ | mean pore diameter |
| $D$ | diffusion coefficient (cm$^2$ s$^{-1}$) |
| $D_b$ | characteristic droplet size (cm) |
| $F$ | Faraday's constant |
| $h$ | water droplet height (cm) |
| $J$ | reaction rate |
| $K$ | constant for droplet size |
| $M$ | molar mass (kg mol$^{-1}$) |
| $M_l$ | interface force of liquid (N) |
| $M_g$ | interface force of gas (N) |
| $n$ | number of electrons |
| $P$ | pressure (Pa) |
| $q$ | switch function |
| $R$ | universal gas constant (J mol$^{-1}$ K$^{-1}$) |
| $Re$ | Reynold number |
| $s$ | water saturation |
| $T$ | temperature (K) |
| $U$ | velocity (cm/s) |
| $V_{cell}$ | cell voltage (V) |
| $V_{oc}$ | open circuit voltage (V) |
| $x$ | mass fraction |
| $y$ | molar fraction |

*Greek letters*

| | |
|---|---|
| $\varepsilon$ | volume fraction |
| $\phi$ | potential (V) |
| $\lambda$ | polymer water content $H_2O/SO_3$ |
| $\mu$ | viscosity (Pa s) |
| $\theta$ | equilibrium contact angle on diffuser |
| $\rho$ | density (kg cm$^{-3}$) |
| $\sigma$ | surface tension (N cm$^{-1}$) |

*Subscripts*

| | |
|---|---|
| a | anode |
| c | cathode |
| C | about capillary |
| d | diffusion layer |
| Darcy | Darcy pressure loss |
| e | about electron |
| g | gas phase |
| $H_2$ | hydrogen |
| i | note for species |
| j | note for species |
| l | liquid phase |
| m | polymer phase |
| mix | gas mixture |
| $O_2$ | oxygen |
| R | relative |
| w | water |
| wd | water dissolved in polymer |
| wp | water production |
| wv | water vapor |

*Superscripts*

| | |
|---|---|
| D | drag force |
| eff | effective |
| L | lift force |
| p | polymer |
| ref | reference |
| sat | water saturated |

simulated the function of a microporous layer between cathode GDL and catalyst layer with the mixture model. Meng and Wang [13] have developed an experimental submodel to consider liquid coverage at the GDL/gas channel interface. In the present work, the size of liquid water droplet detached from the GDL/gas channel interface is considered, which has effect on the liquid removal in the channel and involves the properties of GDL/gas channel interface such as contact angle, surface tension, average pore size of GDL and so on. A two-fluid (TF) model is employed to model liquid water droplet transport in the gas channel, the effect of GDL/gas channel interface properties on the two-phase behavior in the gas channel and GDL is investigated.

## 2. Model development

### 2.1. Model assumptions

The calculated regions consist of conventional channels, gas diffusion electrodes, catalyst layers and a membrane, which are shown in Fig. 1. Because PEMFC is operated in temperature below 100 °C and above normal pressure, so it is assumed that water is generated in cathode catalyst layer as liquid. When water vapor concentration in GDL or gas channel is less than the saturated concentration, liquid water evaporates to vapor, otherwise, water retains a liquid state. The liquid water transfers within the GDL by capillary force, then the liquid water droplet emerges and grows on the GDL/gas channel interface. When the drag force acting on the droplet equal to the adhering force, the droplet obtains the maximum droplet size, then it begins to move on the GDL/gas channel interface or goes into the gas channel. The liquid water is treated as a continuous phase in the form of droplet. To hold up this approach, necessary assumption should be made, i.e. when the droplet detaches from GDL surface by gas shear flow, the effect of gas channel wall's properties (i.e. hydrophobicity) are not considered. However, it is more reasonable for higher gas velocity or small droplet size, and Wang and co-workers [5] suggested that for a gas flow channel with the height of 0.5 mm, when the droplet diameter exceeds 0.2 mm, the droplet may interact with gas flow channel walls. In addition, isothermal condition is also assumed to PEMFCs and gas mixture both in cathode and anode are treated as perfect gas.

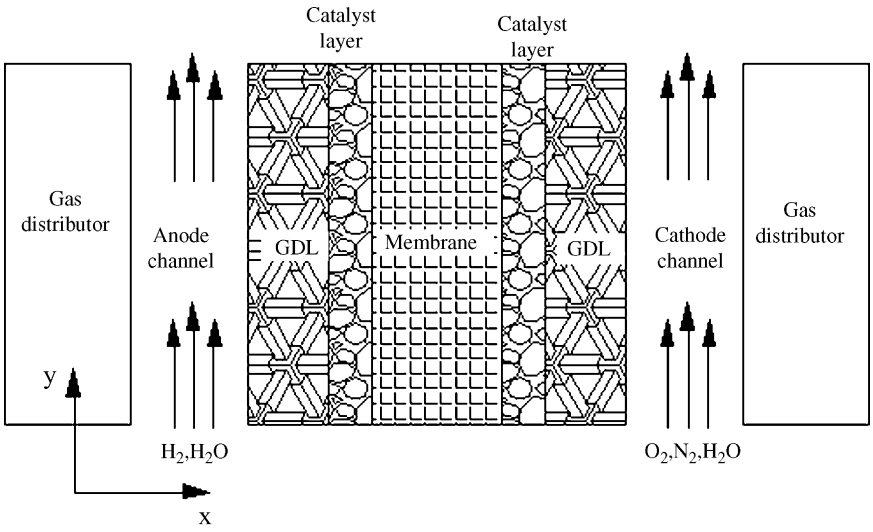


Fig. 1. Calculated domain of PEMFCs.

### 2.2. Governing equations

A two-dimensional two-fluid model is used to describe two-phase flow behavior in a PEMFC gas channel. It considers the flow of gas and liquid phase, respectively. Terms accounting for the interacting force are added into the N-S equations. In the channel, the pressure of the two phases is assumed to be equal. In porous electrodes, the difference of the pressure depends on the capillary force, which is calculated from the Leverett J-function.

Eqs. (1)–(12) in Table 1 contain the governing equations for two-dimensional two-fluid model of PEMFCs, which include conservation of mass, momentum, ionic charge and species. Eqs. (1) and (10) describe the conservation of mass of gas in cathode and anode, respectively. The mass conservation of liquid phase is described by Eqs. (5) and (7) for liquid in cathode gas channel and GDL, respectively. Eqs. (2), (6) and (11) describe the momentum transfer for gas phase in cathode, liquid phase in cathode and gas in anode, respectively. The drag force and lift force between gas phase and liquid phase are considered in gas channel in Eqs. (2) and (6). Eqs. (3) and (12) describe the conservation of water vapor of cathode gas and anode gas, respectively. And the conservation of oxygen is given in Eq. (4). The conservation of ionic charge and water within polymer phase are expressed in Eqs. (8) and (9), respectively. Source terms reflect the mass exchange among liquid phase, gas phase and polymer phase as well as the consumption of reactant by electrochemical reaction are given in Table 2. Parameters used in the equations are listed in Table 3.

### 2.3. The simplified model for calculating the droplet detachment diameter

In PEMFCs, liquid water is produced in cathode catalyst layer and moves out of the gas diffuser by capillary-driven, and then

Table 1
Governing equations

| Phase | Conservation equation | General form | |
|---|---|---|---|
| Cathode gas | Mass | $\nabla(\varepsilon(1-s)\rho_g U_g) = r_w + S_{O_2} - s_{wd} q_{wd}$ | (1) |
| Cathode gas | Momentum | $\nabla[\varepsilon(1-s)\rho_g U_g U_g] = -\varepsilon(1-s)\nabla p_g + \nabla[(1-s)\mu_g \nabla U_g] + \varepsilon\rho_g g + S_{Darcy,g} + M_g^D + M_g^L$ | (2) |
| Cathode gas | Species | $\nabla[\varepsilon(1-s)\rho_g U_g x_{O_2}] = D_{O_2}^{eff}\nabla y_{O_2} + S_{O_2}$ | (3) |
| | | $\nabla[\varepsilon(1-s)\rho_g U_g x_{wv}] = D_{wv}^{eff}\nabla y_{wv} + r_w + q_{wd} S_{wd}$ | (4) |
| Cathode liquid (channel) | Mass | $\nabla(\varepsilon s\rho_l U_l) = -r_w$ | (5) |
| Cathode liquid (channel) | Momentum | $\nabla(\varepsilon s\rho_l U_l U_l) = -\varepsilon s\nabla p_l + \nabla(\varepsilon s\mu_l \nabla U_l) + S_{Darcy,l} + M_l^D + M_l^L$ | (6) |
| Cathode liquid (electrode) | Mass | $\nabla(\varepsilon s\rho_l U_l) = \nabla\left(-\varepsilon s\rho_l \frac{k_l}{\mu_l}\nabla(p_g - p_c)\right) = -r_w + s_{wp} - (1-q_{wd})s_{wd}$ | (7) |
| Polymer phase | Current | $\nabla(K_m \nabla\phi_m) = \begin{cases} J_a & \text{anode catalyst layer} \\ 0 & \text{membrane} \\ J_c & \text{cathode catalyst layer} \end{cases}$ | (8) |
| Polymer phase water | Mass | $\nabla(-D_w\nabla C_w + \lambda\frac{2.5i}{22F} + C_w U) = \begin{cases} (1-q_{wd})\frac{S_{wd}}{M_w} & \text{catalyst layer} \\ 0 & \text{membrane} \end{cases}$ | (9) |
| Anode gas | Mass | $\nabla(\varepsilon\rho U) = S_{H_2} - q_{wd} S_{wd}$ | (10) |
| Anode gas | Momentum | $\nabla(\varepsilon\rho UU) = -\varepsilon\nabla p + \nabla(\varepsilon\mu\nabla U) + \varepsilon\rho g + S_{Darcy}$ | (11) |
| Anode gas | Species | $\nabla[\varepsilon\rho U x_{wv}] = \nabla(\rho D_{w-H_2}^{eff}\nabla x_{wv}) - q_{wd} S_{wd}$ | (12) |

Table 2
Source terms in governing equations

| Source terms (zero in other region) | Defining equation | |
|---|---|---|
| Oxygen reaction rate (cathode catalyst layer) | $S_{O_2} = -J_c \frac{M_{O_2}}{4F}$ | (13) |
| Hydrogen reaction rate (anode catalyst layer) | $S_{H_2} = -J_a \frac{M_{H_2}}{2F}$ | (14) |
| Mass transfer rate between gas and liquid [14] | $r_w = M_w \left[ k_c \frac{\varepsilon(1-s)y_w}{RT}(y_w p - p_w^{sat})q + k_e \varepsilon s C_w (y_w p - p_w^{sat})(1-q) \right]$ | (15) |
| Mass transfer rate between gas and polymer $S_{wd}$ | $h_m(\rho_w^g - \rho_w^p)$ | (16) |
| Darcy pressure drop of gas in cathode and anode $S_{Darcy,g}$ | $-\varepsilon \frac{\mu_g}{K_p(1-s)^3} U_g$ | (17) |
| Darcy pressure drop of liquid in cathode $S_{Darcy,l}$ | $-\varepsilon \frac{\mu_l}{K_p s^3} U_l$ | (18) |
| Liquid generation rate in cathode catalyst layer | $S_{wp} = \frac{J_c}{2F} M_w$ | (19) |

Table 3
Parameters in governing equations

| Parameters | Defining equation | |
|---|---|---|
| Reaction rate in cathode | $J_c = (1-s) A_v i_{0,c}^{ref} \left( \frac{C_{O_2,m}}{C_{O_2}^{ref}} \right) \left[ \exp\left( \frac{-n\alpha_a}{RT}(\phi_m + V_{cell} - V_{oc}) \right) - \exp\left( \frac{n\alpha_c}{RT}(\phi_m + V_{cell} - V_{oc}) \right) \right]$ | (20) |
| Reaction rate in anode | $J_a = A_v i_{0,a}^{ref} \left( \frac{C_{H_2,m}}{C_{H_2}^{ref}} \right) \left[ \exp\left( \frac{-n\alpha_a}{RT}(\phi_e - \phi_m) \right) - \exp\left( \frac{n\alpha_c}{RT}(\phi_e - \phi_m) \right) \right]$ | (21) |
| Polymer phase conductivity | $K_m = (0.005139\lambda - 0.00326) \exp\left[ 1268 \left( \frac{1}{303} - \frac{1}{T} \right) \right] \quad (\lambda > 1)$ | (22) |
| Water content in polymer phase | $C_w = \frac{e\lambda}{f\lambda + 1}$ | (23) |
| Water index in polymer | $\lambda = 0.043 + 17.81a - 39.85a^2 + 36.0a^3$ | (24) |
| Water activity | $a = \frac{x_w p}{p_w^{sat}} \frac{M_{mix}}{M_w}$ | (25) |
| Liquid/vapor switch function | $q = 0.5 + \frac{abs(p_w^{sat} - y_w p + 1e-30)}{2(p_w^{sat} - y_w p + 1e-30)}$ | (26) |
| Gas/polymer switch function | $q_{dw} = 0.5 + \frac{abs(\rho_w^g - \rho_w^p + 1e-30)}{2(\rho_w^g - \rho_w^p + 1e-30)}$ | (27) |
| Water diffusivity in polymer phase [15] | $D_w = 10^{-10} \exp\left[ 2416 \left( \frac{1}{303} - \frac{1}{T} \right) \right] (2.563 - 0.33\lambda + 0.0264\lambda^2 - 0.000671\lambda^3), \quad \lambda > 4$<br>$D_w = 10^{-10} \exp\left[ 2416 \left( \frac{1}{303} - \frac{1}{T} \right) \right] (-1.25\lambda + 6.65), \quad 3 < \lambda \le 4$<br>$D_w = 10^{-10} \exp\left[ 2416 \left( \frac{1}{303} - \frac{1}{T} \right) \right] (2.05\lambda - 3.25), \quad 2 < \lambda \le 3$ | (28) |
| Gas density in cathode | $\rho = \frac{p}{RT} \frac{1}{x_{O_2}/M_{O_2} + x_{wv}/M_w + (1 - x_{O_2} - x_{wv})/M_{N_2}}$ | (29) |
| Gas density in anode | $\rho = \frac{p}{RT} \frac{1}{(1 - x_{wv})/M_{H_2} + x_{wv}/M_w}$ | (30) |
| Gas diffusivity [16] | $D_{AB} = \frac{1}{p} 0.000364 \left( \frac{T}{\sqrt{T_{CA} T_{CB}}} \right)^{2.334} (p_{CA} p_{CB})^{1/3} (T_{CA} T_{CB})^{5/12} \left( \frac{1}{M_A} + \frac{1}{M_B} \right)^{1/2}$<br>$D_k = \frac{\rho_g (1 - y_k)}{RT \sum_{j \ne k} (y_j / D_{jk})}, \qquad D_{AB}^{eff} = D_{AB}[\varepsilon(1-s)]^{1.5}$<br>$\varepsilon = 1$ for channel $\varepsilon$ = GDL porosity in GDL, otherwise $\varepsilon$ = catalyst layer porosity | (31) |
| Drag force between liquid and gas [17] | $M_g^D = -M_l^D = 0.75 C_D \frac{\rho_g}{D_b} s \lvert U_R \rvert U_R$ | (32) |
| Drag coefficient [18] | $C_D = \frac{24}{Re}(1 + 0.1925 Re^{0.63})$ | (33) |
| Relative velocity | $U_R = U_l - U_g$ | (34) |
| Reynold number | $Re = (1-s) \frac{\rho_g D_b \lvert U_R \rvert}{\mu_g}$ | (35) |
| Lift force [19] | $M_l^L = -M_g^L = C_L \rho_g s U_R (\nabla U_g)$ | (36) |
| Lift coefficient | $C_L = C_{La}(1 - 2.78(0.2, s))$ | (37) |
| Capillary pressure | $p_C = p_g - p_l = \sigma \cos\theta \left( \frac{\varepsilon}{K_p} \right)^{1/2} J(s)$ | (38) |
| Leverett J-function [10] | $J(s) = \begin{cases} 1.417(1-s) - 2.120(1-s)^2 + 1.263(1-s)^3, & \text{if } \theta_C < 90^\circ \text{ hydrophilic media} \\ 1.417s - 2.120s^2 + 1.263s^3, & \text{if } \theta_C > 90^\circ \text{ hydrophobic media} \end{cases}$ | (39) |

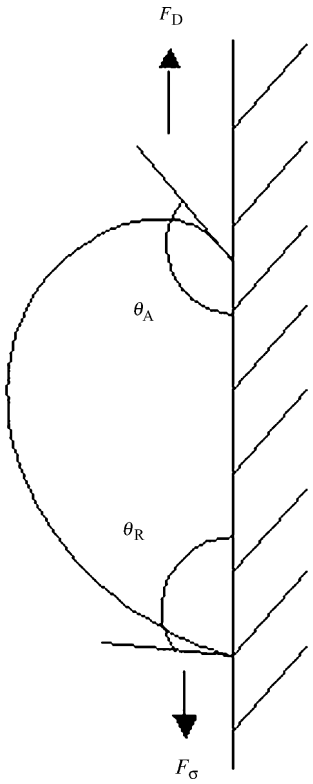


Fig. 2. Schematic view of a droplet on the GDL/channel interface.

liquid water drop is formed on the GDL/gas channel interface. As mentioned above in Section 2.1, the water droplet detachment diameter is determined by the surface tension force and drag force acting on the droplet on GDL surface shown in Fig. 2. The surface tension force along surface direction is:

$$F_\sigma = 2\int_0^\pi \sigma \cos\theta \cos\beta \left(\frac{d_c}{2}\right) d\beta \tag{40}$$

Here, $\theta_A$ and $\theta_R$ are the advancing angle and receding angle, respectively, $\sigma$ the surface tension and $\theta$ is the contact angle. Its value varies from $\theta_R$ to $\theta_A$ corresponding to the angle $\beta$ from 0 to $\pi$. Assuming the value of $\theta$ changes from $\theta_R$ to $\theta_A$ periodically:

$$\theta = \frac{\beta(\theta_A - \theta_R)}{\pi + \theta_R} \tag{41}$$

Integrating Eq. (40), we have

$$F_\sigma = \frac{\sigma d_c}{2}\pi(\sin\theta_A + \sin\theta_R) \times \left(\frac{1}{\pi - (\theta_A - \theta_R)} - \frac{1}{\pi + (\theta_A - \theta_R)}\right) \tag{42}$$

Here, $d_c$ is the contact diameter between liquid and solid phase. For a solid surface, $d_c$ can be obtained according to the droplet diameter $d$ and the contact angle as:

$$d_c = d \sin\left(\frac{\theta_A + \theta_R}{2}\right) \tag{43}$$

But in the case of GDL in PEMFCs, the liquid water droplet is formed on the GDL surface by the accumulation of the water flowing out the GDL through the pores. So, the initial contact diameter between the liquid water and the solid phase equal the diameter of the pores. With the droplet growing, the contact diameter will be unchanged until coalescence happens between neighboring droplets. However, the liquid water droplets appear only at the some preferential positions but not on the whole surface [3], so, coalescence is not considered in the present work, and the contact diameter in this study is assigned to be the mean pore diameter in GDL.

For a droplet on the surface in the shear flow, specifying the value of $\theta_R$ and $\theta_A$ is the key problem and also is very difficult. They change with the gas velocity, viscosity ratio, etc. [20,21]. To simplify the calculation, the critical value of $\theta_R$ and $\theta_A$ for a liquid drop on an inclined PTFE plane are used for all the cases. For a PTFE surface [22],

$$\frac{\theta_A - \theta_R}{\theta_A} = 0.2 \tag{44}$$

Assuming $\theta_R$ and $\theta_A$ are symmetric by the static contact angle $\theta_s$.

$$\frac{\Delta\theta}{\theta_s - \Delta\theta/2} = 0.2 \tag{45}$$

For the static contact angle of liquid water on TGPH-090 surface with 10 wt.% FEP treated, Wang and co-workers [23] have measured it with the value of 80° under 80 °C and approximately 100° under 20 °C.

The drag force on the droplet by the gas flow along the surface direction is

$$F_D = \int_{\pi-\theta_M}^{\pi} \frac{v^2}{2} C_D \rho_g \frac{1}{2}\left(\frac{d}{\sin(\pi - \theta_M)}\right)^2 \sin^2\beta \, d\beta \tag{46}$$

where

$$\theta_M = \frac{\theta_A + \theta_R}{2} \tag{47}$$

$C_D$ is the drag force coefficient, which can be estimated by

$$C_D = \frac{24}{Re}(1 + 0.1925 Re^{0.63}) \tag{48}$$

where $Re$ is defined as

$$Re = \frac{\rho_g v d}{\mu_g} \tag{49}$$

And the fully developed laminar flow velocity distribution in a rectangular enclosure can be represented by [24]

$$v(y) = \frac{3}{2} v_c \left[1 - \left(\frac{2y}{B}\right)^2\right] \tag{50}$$

where $v(y)$ is the vertical velocity, $B$ the channel height, $v_c$ the average gas velocity in the channel and $y$ represents the distance to the channel central line.

Table 4
Boundary conditions

| Equations | Inlet | Outlet | Wall |
|---|---|---|---|
| Anode momentum | $v = 600\,\text{cm/s}$, $u = 0$, $p = 0.2\,\text{MPa}$ | Fully developed | $v = 0$, $u = 0$ |
| Anode water vapor | $x_{wv} = 0.7513$ | $\nabla x_{wv} = 0$ | $\nabla x_{wv} = 0$ |
| Cathode gas momentum | $v_c = 700\,\text{cm/s}$, $u = 0$, $p = 0.2\,\text{MPa}$ | Fully developed | $v = 0$, $u = 0$ |
| Cathode water vapor | $x_{wv} = 0.159$ | $\nabla x_{wv} = 0$ | $\nabla x_{wv} = 0$ |
| Cathode oxygen | $x_{O_2} = 0.195$ | $\nabla x_{O_2} = 0$ | $\nabla x_{O_2} = 0$ |
| Cathode liquid momentum | $u = 0$; $v = 0$; $p = 0.2\,\text{MPa}$ | Fully developed | $v = 0$, $u = 0$ |
| Cathode liquid saturation | $s = 0$ | $\nabla s = 0$ | $\nabla s = 0$ |

In this work, gravity is neglected, so the droplet shown in Fig. 2 is equivalent to the droplet on the horizontal surface, and this is the same situation in Wang's experiment [5].

## 3. Boundary conditions and numerical method

Boundary conditions used in the model are given in Table 4. Since the model is solved by an iterative solution technique, the starting solution can affect the convergence and computing time. The starting solution for the species here was set to be equal to their respective inlet boundary values. The collector plates, membrane are impermeable for species and the GDL is impermeable for proton. Table 5 gives the values of parameters.

Because the thickness of channel, diffusion layer, catalyst layer and membrane differ much, the non-uniform mesh grid is used. There are 20 mesh grids in channel, 10 mesh grids in GDL, 5 mesh grids in the catalyst layer, 20 mesh grids in the membrane and 450 mesh grids along the channel ($y$-direction). The governing equations were solved by our C language code using iterative method. The Simple Algorithm [26] is used to solve single phase flow in anode, and Inter-Phase Slip Algorithm (IPSA) is used to solve two-phase floe in cathode. When the relative error of all variables between two iterations are less than 1e−4, it is considered to reach a convergence. A sensitive analysis was conducted by doubling the number of mesh grids. The solution difference on average is less than 3%, so it was assumed to be mesh grid independent.

Table 5
Value of parameters

| Physical properties | Value |
|---|---|
| Faraday's constant, $F$ ($\text{C mol}^{-1}$) | 96,487 |
| Permeability of gas diffusion layer, $K_p$ ($\text{cm}^2$) | $8 \times 10^{-8}$ |
| Cathode gas viscosity, $\mu_c$ (Pa s) | $2.0 \times 10^{-5}$ |
| Anode gas viscosity, $\mu_a$ (Pa s) | $2.0 \times 10^{-5}$ |
| Liquid water viscosity, $\mu_l$ (Pa s) | $3.565 \times 10^{-4}$ |
| Anodic transfer coefficient, $\alpha_a$ | 0.5 |
| Cathodic transfer coefficient, $\alpha_c$ | 0.55 |
| Water contact angle in diffuser, $\theta$ (°) | 120 |
| Gas channel width (cm) | 0.05 |
| Gas channel length (cm) | 40 |
| Gas channel height (cm) | 0.05 |
| Anode GDL thickness (cm) | 0.018 |
| Cathode GDL thickness (cm) | 0.018 |
| Gas diffusion layer void fraction | 0.7 |
| Catalyst layer thickness (cm) | 0.001 |
| Catalyst layer void fraction | 0.6 |
| Average pore size in GDL (μm) | 23 [25] |
| Membrane thickness (Nafion®115) | 0.0127 |
| Cell temperature (K) | 353 |
| Inlet pressure (MPa) | 0.2 |
| Air inlet relative humidity (%) | 100 |
| Fuel inlet relative humidity (%) | 100 |
| Open circuit voltage (V) | 1.17 |
| Operation voltage (V) | 0.55 |
| Evap./cond. mass transfer coefficient $k_e$, $k_c$ ($\text{kg cm}^{-3}\,\text{s}^{-1}$) | 2 [6] |
| Dissolved/vapor mass transfer coefficient, $h_m$ ($\text{s}^{-1}$) | 5000 [6] |
| Reference kinetic parameter in cathode, $A_v i_{0,c}^{ref}$ ($\text{A cm}^{-3}$) | $1.1 \times 10^{-6}$ |
| Reference kinetic parameter in anode, $A_v i_{0,a}^{ref}$ ($\text{A cm}^{-3}$) | $1.5 \times 10^{5}$ |
| Water surface tension, $\sigma$ ($\text{N m}^{-1}$) | 0.0625 |

## 4. Results and discussion

### 4.1. Model validation

To validate the model above, firstly, the predicted droplet detachment diameter is compared with the experimental data by Wang [5], which is a very important factor in the TF model presented in this study. Fig. 3 shows the comparison between calculated detachment diameter by our simplified model and Wang's experimental data, and they agree pretty well. This validates the simplified model. Second, the comparison between the predicted fuel cell performance and our experimental data also have been presented in Fig. 4 for different operation pressures. Good agreement is obtained, so the present model is demonstrated to be accurate.

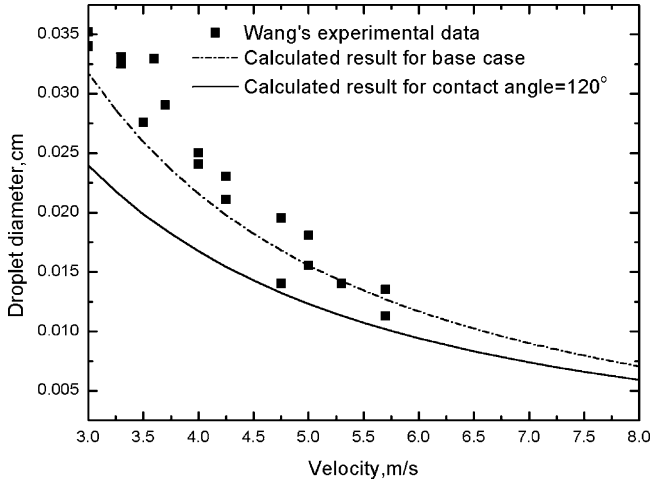


Fig. 3. Comparison between predicted droplet diameter and experimental data.

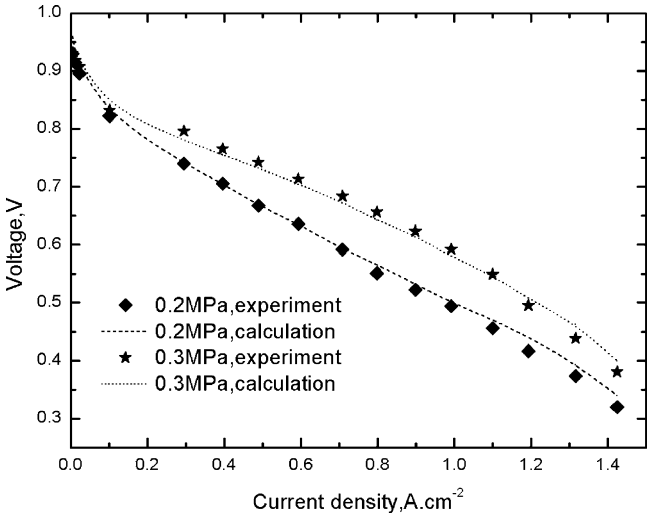


Fig. 4. Comparison between numerical performance of PEMFC and experiment data for different operating pressures.

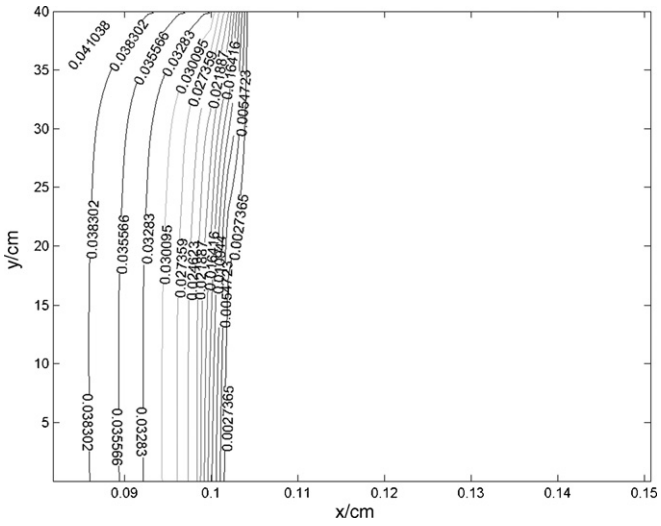


Fig. 6. Saturation in GDL and channel for contact angle on GDL/channel interface equal to 120°.

### 4.2. Effect of GDL/channel interface hydrophobicity on droplet detachment diameter and water saturation distribution in GDL

There are also results of predicted detachment diameter for different contact angle (80°, 120°) on the GDL surface in Fig. 3. The results show that with the increases of contact angle on GDL surface, the detachment diameter decreases. Figs. 5 and 6 show the water saturation in GDL for the base case and the contact angle on GDL surface equal to 120°. For both cases, the water saturation increases from inlet to outlet in vertical direction and from channel to catalyst layer in horizontal direction. This is consistent with the observation results by Yang [3]. On the GDL/channel interface, the water saturation increases from inlet to outlet. It can be demonstrated by the fact that with gas flows from inlet to outlet and liquid water moves through GDL to GDL/channel interface, more and more water droplets are dragged by the gas and travels with acceleration in the channel. So the space on the GDL/channel interface occupied by the liquid water increases. Comparing Fig. 5 with Fig. 6, it is obvious that the water saturation for base case is larger than that of 120° case. According to Fig. 3, large contact angle on GDL/channel interface produces small detaching droplet, so small droplet travels by drag force easily. When the droplet is small enough, the droplet will move at the same velocity as gas, and the efficient removal of liquid water can be obtained. So high contact angle on GDL/channel interface is advantageous for water removal in GDL and gas channel.

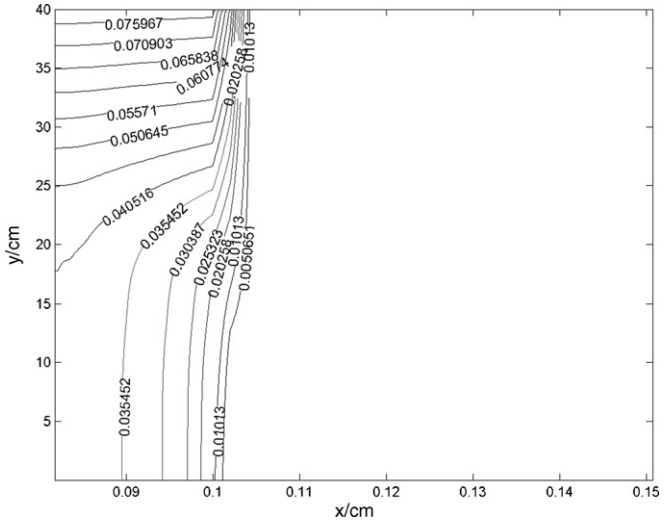


Fig. 5. Saturation in GDL and channel for base case.

### 4.3. Effect of water surface tension on droplet detachment diameter and water saturation distribution in GDL

According to Eq. (40), the adhering force is proportional to the surface tension. Fig. 7 shows the droplet detachment diameter for normal water surface tension, 80% of the water surface tension and 120% of the water surface tension. The detach-

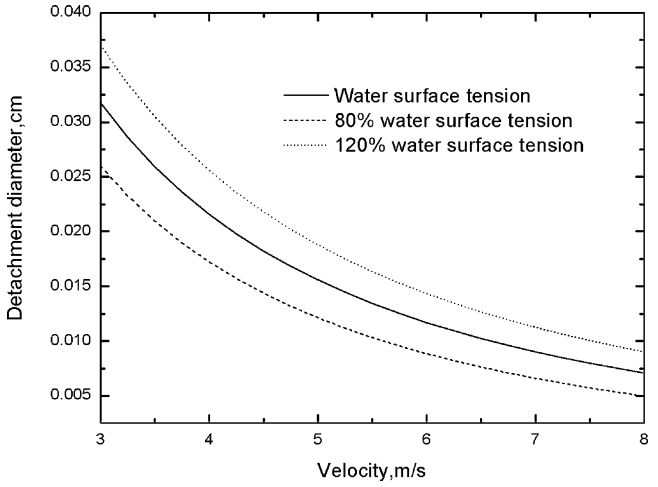


Fig. 7. Predicted detachment diameter for different surface tension.

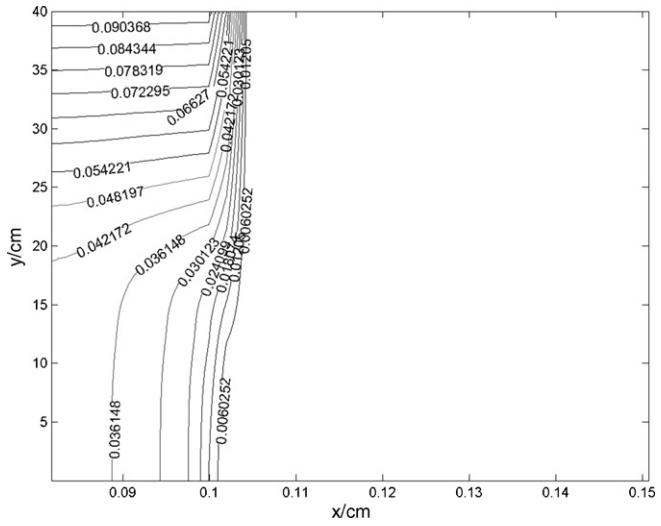


Fig. 8. Saturation in GDL and channel for 80% of water surface tension in GDL.

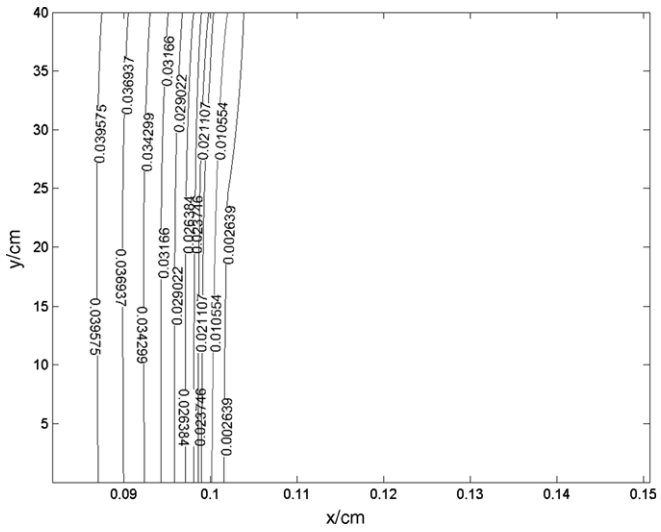


Fig. 10. Saturation in GDL and channel for 80% of water surface tension both in GDL and on GDL/channel interface.

ment diameter obviously increases with the increase of surface tension. From this point of view, reducing the surface tension may be a way to enhance liquid water removal on GDL/channel interface. However, as shown in Eq. (38), reducing surface tension may decrease the capillary pressure in GDL, which is the dominating force for liquid flow in GDL. In this way, reducing surface tension may cause liquid water accumulation in GDL, which is demonstrated by the numerical results shown in Figs. 8 and 9, where the water saturation in GDL for 80% of the water surface tension in GDL and 120% of the water surface tension in GDL are given, respectively, but the value of surface tension used to calculate the droplet detachment diameter retains original value. It is obvious that decreasing surface tension in GDL causes serious saturation in GDL, and this is disadvantageous for liquid removal. To investigate the final effect of surface tension (both in GDL and on GDL/channel interface) on the water removal, numerical simulation has been done. Figs. 10 and 11 show the water saturation in GDL for 80 and 120% of the water surface tension (both in GDL and on GDL/channel interface), respectively. It can be seen that water saturation in GDL for 80% of water surface tension is largely decreased compared with the result in Fig. 5. Along the GDL/channel interface, the saturation changes slightly, which means that the droplet moves faster for small ones, thus, only a few spaces on GDL/channel interface are occupied by the droplet. In Fig. 11, although the capillary pressure in GDL increases due to the increase of surface tension, the droplet on GDL/channel interface cannot be easily dragged by the gas due to the large size. It is the cause of the accumulation of liquid on GDL/channel interface, and correspondingly, it hinders the liquid water transfer from catalyst layer to GDL/channel interface. Saturation in GDL increases too. Fig. 12 shows the current density along the y direction on cathode catalyst layer/membrane interface for 80 and 120% of the water surface tension. It indi-

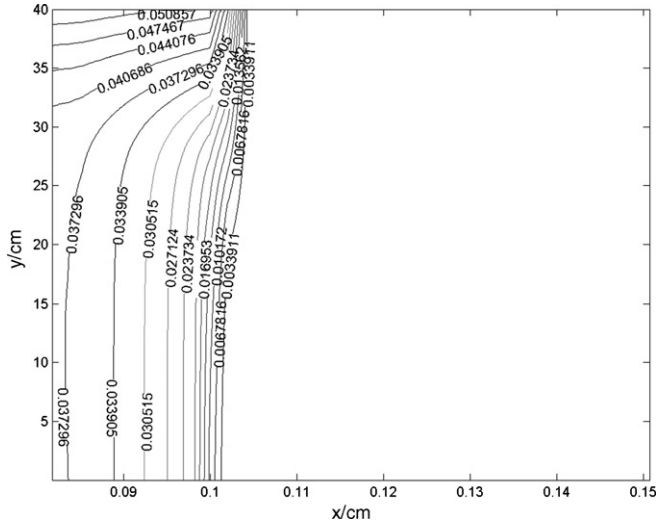


Fig. 9. Saturation in GDL and channel for 120% of water surface tension in GDL.

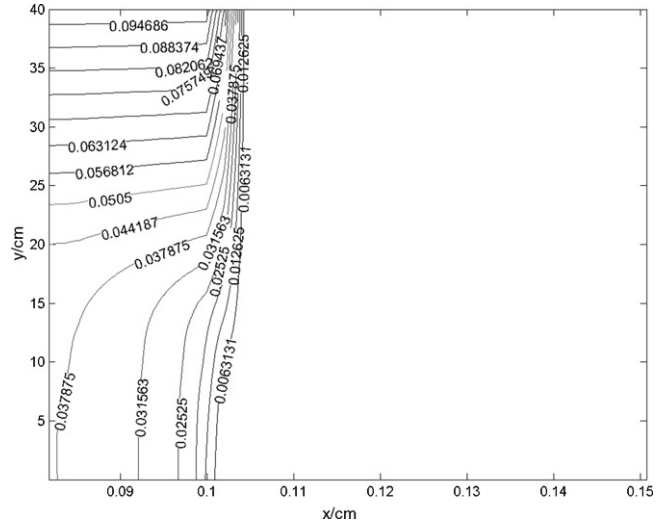


Fig. 11. Saturation in GDL and channel for 120% of water surface tension both in GDL and on GDL/channel interface.

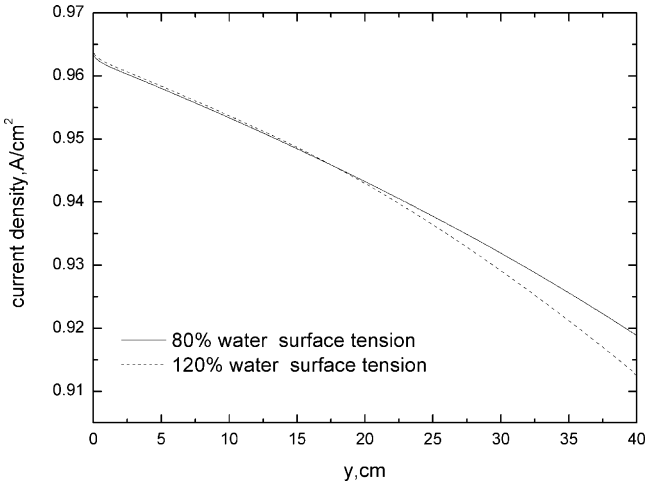


Fig. 12. Current density on cathode catalyst layer/membrane interface for 80 and 120% of water surface tension.

cates that there is hardly any difference in the upstream section for two cases, but for downstream section, due to the high saturation of 120% of surface tension case, the current density is obvious lower than that of 80% case. According to the result above, it can be concluded that increasing surface tension is disadvantageous for liquid removal in the GDL and channel.

### 4.4. Oxygen mass fraction in cathode

Figs. 13 and 14 show the oxygen fraction distribution in cathode channel, GDL and catalyst layer for base case and the operation voltage equal to 0.4 V. It indicates that the oxygen mass fraction decreases from inlet to outlet and from channel to catalyst layer. In addition, with the decreases of operation voltage (i.e. increases of current density), the consumption of oxygen increases, and the minimum oxygen mass fraction appears at the inner of downstream section.

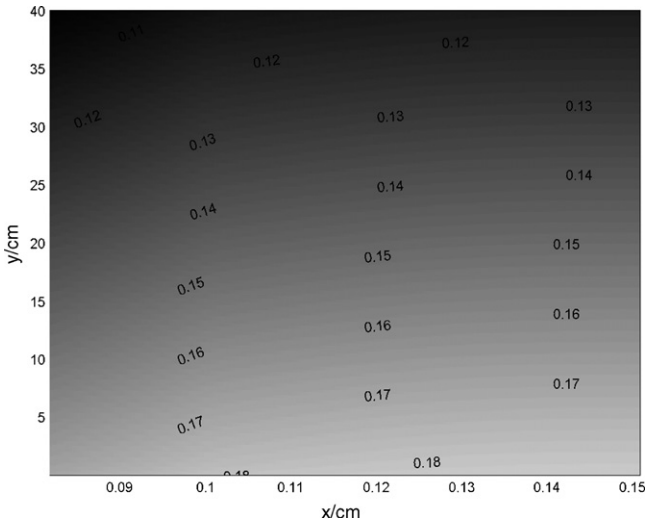


Fig. 13. Oxygen mass fraction in cathode channel, GDL and catalyst layer for base case.

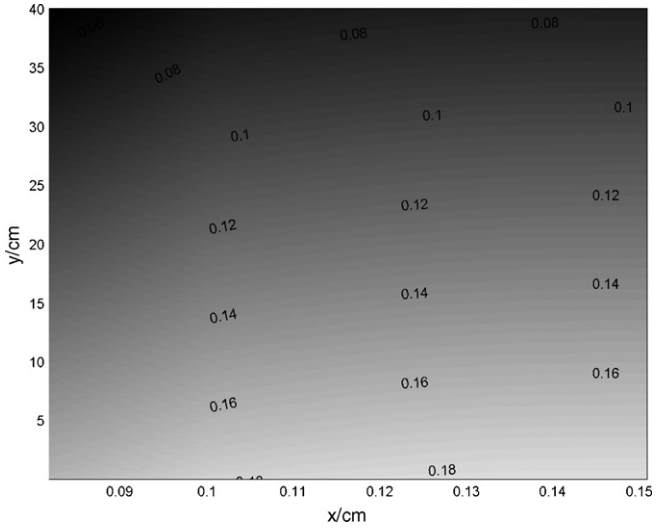


Fig. 14. Oxygen mass fraction in cathode channel, GDL and catalyst layer for 0.4 V of operation voltage.

## 5. Conclusion

In this paper, a two-dimensional two-fluid (TF) model is developed to simulate the two-phase flow behavior in PEMFCs. A simplied model is also applied to predict the detachment diameter of the liquid droplet at the GDL/channel interface. The effect of the GDL/channel interface properties (contact angle, surface tension) on the two-phase behavior was mainly investigated, and the conclusions are:

(1) A high contact angle of the liquid water at the GDL/channel interface produces a small detaching liquid droplet, and enhances water removal at the GDL/channel interface and in the GDL, which is advantageous for PEMFC operation.
(2) A low surface tension produces a small detaching liquid droplet, which is advantageous for water removal in the channel and the GDL, even though a low surface tension decreases the capillary force in the GDL. In contrast, high surface tension hinders liquid removal from the GDL/channel interface, which is disadvantageous for PEMFC operation, even though it enhances the capillary force in the GDL.

In this work, the two-phase flow behavior at the anode is not considered, because it is not significant unless the anode is severely flooded. The hydrophobicity or hydrophilicity of the gas channel walls also have effects on water removal, especially for large liquid droplets, and a further study will be done in future.

## References

[1] K. Tüber, D. Pócza, C. Hebling, Visualization of water buildup in the cathode of a transparent PEM fuel cell, J. Power Sources 124 (2003) 403–414.
[2] A. Hakenjos, H. Muenter, U. Wittstadt, C. Hebling, A PEM fuel cell for combined measurement of current and temperature distribution, and flow field flooding, J. Power Sources 131 (2004) 213–216.

[3] X.G. Yang, F.Y. Zhang, A.L. Lubawy, C.Y. Wang, Visualization of liquid water transport in a PEFC, Electrochem. Solid-State Lett. 7 (2004) A408–A411.
[4] P.K. Sinha, P. Halleck, C.Y. Wang, Quantification of liquid water saturation in a PEM fuel cell diffusion medium using X-ray microtomography, Electrochem. Solid-State Lett. 9 (2006) A344–A348.
[5] F.Y. Zhang, X.G. Yang, C.Y. Wang, Liquid water removal from a polymer electrolyte fuel cell, J. Electrochem. Soc. 153 (2006) A225–A232.
[6] W. He, J.S. Yi, T. Van Nguye, Two-phase flow model of the cathode of PEM fuel cell using interdigited flow fields, AICHE J. 10 (2000) 2053–2064.
[7] N.P. Siegel, M.W. Ellis, D.J. Nelson, M.R. von Spakovsky, A two-dimensional computational model of a PEMFC with liquid water transport, J. Power Sources 128 (2004) 173–184.
[8] L. You, H. Liu, A two-phase flow and transport model for the cathode of PEM fuel cells, Int. J. Heat Mass Transfer 45 (2002) 2277–2287.
[9] L. You, H. Liu, A two-phase flow and transport model for PEM fuel cells, J. Power Sources 155 (2006) 219–230.
[10] H. Sun, H. Liu, L.-J. Guo, PEM fuel cell performance and its two-phase mass transport, J. Power Sources 143 (2005) 125–135.
[11] Z.H. Wang, C.Y. Wang, K.S. Chen, Two-phase flow and transport in the air cathode of proton exchange membrane fuel cells, J. Power Sources 94 (2001) 40–50.
[12] U. Pasaogullari, C.Y. Wang, K.S. Chenb, Two-phase transport in polymer electrolyte fuel cells with bilayer cathode gas diffusion media, J. Electrochem. Soc. 152 (2005) A1574–A1582.
[13] H. Meng, C.-Y. Wang, Model of two-phase flow and flooding dynamics in polymer electrolyte fuel cells, J. Electrochem. Soc. 152 (2005) A1733–A1741.
[14] D. Natarajan, T. van Nguyen, A two-phase, multicomponent, transient model for the cathode of a proton exchange membrane fuel cell using conventional gas distributors, J. Electrochemical. Soc. 148 (2001) A1324–A1335.
[15] T.E. Springer, T.A. Zawodzinski, S. Gottesfeld, Polymer electrolyte fuel cell model, J. Electrochem. Soc. 138 (1991) 2334–2341.
[16] J.M. Stockie, K. Promislow, B.R. Wetton, A finite volume method for multicomponent gas transport in a porous fuel cell electrode, Int. J. Numer. Methods Fluids 41 (2003) 577–599.
[17] M. Shii, K. Mishima, Two-fluid modeling and hydrodynamic constitutive relations, Nucl. Eng. Des. 4 (1984) 107–116.
[18] R. Clift, J.R. Grance, M.E. Weber, Bubbles Drops and Particals, Academic press, New York, 1978.
[19] D.A. Drew, R.T. Lahey, The virtual mass and lift force on a sphere in rotating and straining in viscid flow., Int. J. Multiphase Flow 13 (1987) 113–121.
[20] P. Dimitrakopoulos, J.L. Higdon, Displacement of fluid droplets from solid surfaces in low-Reynolds-number shear flows, J. Fluid Mech. 336 (1997) 351–378.
[21] P. Dimitrakopoulos, J.L. Higdon, On the displacement of three-dimensional fluid droplets adhering to a plane wall in viscous pressure-driven flows, J. Fluid Mech. 435 (2001) 327–350.
[22] C.W. Extrand, Y. Kumagai, An experimental study of contact angle hysteresis, J. Colloid Interface Sci. 191 (1997) 378–383.
[23] C. Lim, C.Y. Wang, Effects of hydrophobic polymer content in GDL on power performance of a PEM fuel cell, Electrochim. Acta 49 (2004) 4149–4156.
[24] F.M. White, Fluid Mechanics, fourth ed., McGraw-Hill Series in Mechanical Engineering, 1999, pp. 357–362.
[25] M. Mathias, J. Roth, J. Fleming, W. Lehnert, Chapter 46: Diffusion media materials and characterization, in: W. Vielstich, H. Gasteiger, A. Lamm (Eds.), Handbook of Fuel Cells—Fundamentals, Technology and Applications, John Wiley & Sons, Ltd., 2003.
[26] S.V. Patankar, Numerical Heat Transfer and Fluid Flow, Hemisphere, NewYork, 1980.